Statistical Learning Over Time-Reversal Space for Indoor Monitoring System

Qinyi Xu, *Student Member, IEEE*, Zoltan Safar, Yi Han, Beibei Wang, *Senior Member, IEEE*, and K. J. Ray Liu, *Fellow, IEEE*

***Abstract*—As embedded in wireless signals, information of an indoor environment is captured during radio propagation, motivating the development of emerging wireless sensing technologies. In this paper, we propose a smart radio system that leverages the informative wireless radios to enable intelligent environment and extend human senses to perceive the world. In particular, owing to the time-reversal (TR) technique that captures changes in multipath profiles, the proposed TR indoor monitoring system (TRIMS) is capable of monitoring indoor events and detecting motion through walls in real time. A statistic model of intraclass TR resonance strength is developed and treated as the feature for TRIMS. Moreover, a prototype of TRIMS is implemented using commercial WiFi devices with three antennas. We investigate the performance of TRIMS in different single family houses with normal resident activities. In general, TRIMS can have a perfect detection rate with almost zero false alarm rates for seven target events, whereas during a two-week experiment TRIMS achieves a detection rate of 95.45% in the indoor multi-event monitoring. The proposed TRIMS illustrates the potential of smart radio applications in smart homes, thanks to the ubiquitous WiFi.**

***Index Terms*—Indoor activity monitoring, real-time monitoring, smart radio, time-reversal (TR).**

I. Introduction

THE DEVELOPMENT of emerging wireless sensing technologies has enabled a plenty of applications that utilizes wireless signals, or more specifically the wireless channel state information (CSI), to perceive and exploit the information hidden in the indoor environment. By deploying wireless transceivers indoors, both macro changes introduced by human activities and moving objects, and micro changes generated by gestures and vital signals, can be extracted from the CSI and recognized through passive wireless sensing.

The feasibility of wireless passive sensing relies on the multipath propagation. Multipath propagation is the phenomenon that a transmitted wireless signal reaches the receiver (RX) through different paths after being reflected and scattered by different objects in the indoor environment. A typical indoor multipath environment is demonstrated in Fig. 1, where the channel between the transmitter (TX) and the RX consists of paths affected by: 1) walls; 2) doors of each room; and 3) a moving human. Hence, as long as the states of an indoor environment changes, the channel will record it in the CSI, enabling the detection of activities by wireless passive sensing.

Existing research on wireless passive sensing can be categorized into different groups based on the features extracted from the wireless channel. To begin with, traditional wireless passive sensing systems are mainly based on the received signal strength (RSS) [1]–[5]. However, due to the fact that the RSS is coarse-grained and can be easily corrupted by multipath effect, RSS-based sensing systems often require a line-of-sight (LOS) transmission, resulting in a limited accuracy in indoor activity detection. In order to improve the accuracy and expand the applicable scenario of traditional wireless passive sensing, a much more informative feature, the CSI, becomes prevalent. Since the CSI is typically of high dimensions, it contains more detailed information and supports fine-grained classification applications, such as human motion detection [6]–[15], and hand motion recognition [16], [17]. Among most of these works, due to the randomness of phase distortion in the CSI, only amplitude of the CSI was used to detect indoor activities, while ignoring the information in the phase. Later, both amplitude and phase information of the CSI was utilized in [7] to detect the dynamics of an indoor environment. However, it can only differentiate between the static and dynamic states in a LOS setting and the phase information was sanitized through linear fitting with notable drawbacks. A home intrusion detection system was proposed in [14] which treated the amplitude of the CSI as the feature. However, there is no study on the false alarm rate and long-term performance for the proposed system. Another category of wireless passive sensing techniques relies on the time-of-flight (ToF) of received signals to track the distance changes of reflected moving objects [18]–[24]. However, in order to extract the fine-grained ToF information, extremely large bandwidths or specially designed frequency-modulated continuous-wave signals are required. Hence, those techniques cannot be implemented on off-the-shelf WiFi devices and their ability of detecting multiple indoor events has not been studied yet.

Recently, thanks to its capability of capturing the difference between different CSI, time-reversal (TR) technique has been applied to wireless event detection in an indoor environment [25]. Even though the proposed system achieved

Manuscript received July 25, 2017; revised November 30, 2017; accepted December 27, 2017. Date of publication January 5, 2018; date of current version April 10, 2018. *(Corresponding author: Qinyi Xu.)*

Q. Xu, Z. Safar, B. Wang, and K. J. R. Liu are with the Department of Electrical and Computer Engineering, University of Maryland at College Park, College Park, MD 20742 USA, and also with Origin Wireless, Inc., Greenbelt, MD 20770 USA (e-mail: qinyixu@umd.edu; zsafar@umd.edu; bebewang@umd.edu; kjrliu@umd.edu).

Y. Han is with Origin Wireless, Inc., Greenbelt, MD 20770 USA (e-mail: yi.han@originwireless.net).

Digital Object Identifier 10.1109/JIOT.2018.2789928

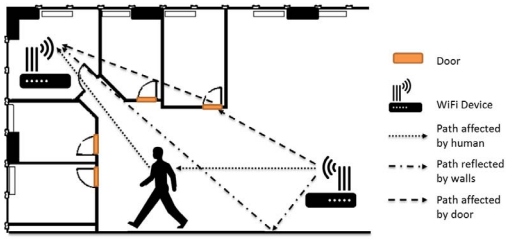

Fig. 1. Illustration of an indoor multipath environment.

an accuracy over 96.9% in detecting multiple events by utilizing information in the complex valued CSI, the system required a transmission under 125-MHz bandwidth which cannot be implemented with commodity WiFi. Moreover, it has no experimental results which evaluates the accuracy in motion detection. Meanwhile, it lacks a long-term study on performance in practical use with critical interference introduced by resident activities.

Given the limitations of the aforementioned studies, we are motivated to develop a new indoor monitoring system that not only can fully utilize the information embedded in multipath channels, but also support simple implementation with commercial WiFi devices while maintaining a high detection accuracy. To achieve this goal, we propose TR-based indoor monitoring system (TRIMS), which utilizes both amplitude and phase information in the CSI obtained from off-the-shelf WiFi devices and succeeds in monitoring indoor environments in real time under both LOS and NLOS sensing scenarios. In particular, TRIMS is implemented on off-the-shelf WiFi devices which operate around 5.8 GHz with 40-MHz bandwidth, and capable of both multievent detection and motion detection. Moreover, unlike the aforementioned works that use the strength of TR resonance (TRRS) directly as a similarity score for recognition and localization, TRIMS relies on the statistical behavior of TRRS to differentiate different events. The statistics of TRRS is derived in this paper and used as features in TRIMS for event detection and motion monitoring. The performance of TRIMS is evaluated through experiments conducted in different single family houses with resident activities. TRIMS is shown to have a high accuracy in monitoring different indoor events and detecting the existence of indoor motion. Furthermore, the accuracy of TRIMS is maintained over 95% during a long-term test lasting for two weeks.

The major contributions of this paper are summarized below.

1) To fully utilize the information in the CSI, both amplitude and phase information is considered. Moreover, we explore the TR technique to capture the difference in the CSI and use the TRRS to quantify the similarity between CSI samples.
2) The statistical behavior of intraclass TRRS is first studied in this paper. The derived statistical model of intraclass TRRS is then served as the feature in the proposed smart radio, TRIMS, to differentiate between different indoor events.
3) Built upon the theoretic analysis, the smart radio, TRIMS, is proposed to monitor indoor environments, recognize different events, and detect the existence of motion in real time. TRIMS is implemented on commodity WiFi devices and evaluated through extensive long-term experiments conducted in real homes with resident activities.

The rest of this paper is organized as follows. We introduce the theoretical foundation of the proposed smart radio system in Section II. Section III presents an overview of the proposed TRIMS as well as the details of both event detector and motion detector in TRIMS. The performance of TRIMS is studied and evaluated in Section IV, where the long-term behavior of TRIMS is also investigated. We briefly discuss the future works as well as the limitations in Section V. This paper is concluded in Section VI.

II. Preliminaries

In this section, the theoretical foundation of the proposed smart radio system, TRIMS, are discussed. We introduce and explain the concept of the TR space where each indoor event is represented by a distinct TR signal. Moreover, we derive the statistics of intraclass TRRS, which later is used as the feature for the event detector in TRIMS.

A. Time-Reversal Resonance

What Is TR Technique? In a rich scattering and reflecting environment, the wireless channels are indeed multipath channels which contain the characteristics of an indoor environment. The evolution of TR technique can be dated back to 1957 [26] when it was proposed to compensate the delay distortion in picture transmission. Later, TR technique has been extended to applications in acoustics [27]–[29] and the electromagnetic (EM) field [30]–[34]. More recently, TR has been advocated as a novel solution for green wireless communication systems and the TR signal transmission was introduced in [35].

The TR signal transmission consists of two phases: 1) channel probing phase during which the CSI $h(t)$ between the TX and the RX is estimated at the TX and 2) data transmission phase during which the TR signature $g(t)$ is convolved with data signals and sent out from the TX to the RX which is the time reversed and conjugated version of $h(t)$. Through TR signal transmission, a spatial-temporal resonance is produced by fully collecting the energy in the multipath channel and concentrating it at the intended location. In physics, the spatial-temporal resonance is the result of a resonance of EM field, in response to the environment. Hence, a strong TR resonance indicates a match between the transmitted TR signature and its propagation channel. In other words, TRRS can be viewed as a similarity measurement between different CSI. TR technique has been utilized in many indoor sensing applications, including indoor locationing [36], indoor human recognition [37], and vital sign monitoring [38].

In Fig. 2, each snapshot of the indoor radio propagation environment, associated with the unique CSI, is represented by a point in the CSI logical space. By taking a TR operation, the corresponding TR signature is generated, mapping each physical indoor events or locations into a new point in the TR space. Since each multipath profile is uniquely determined by

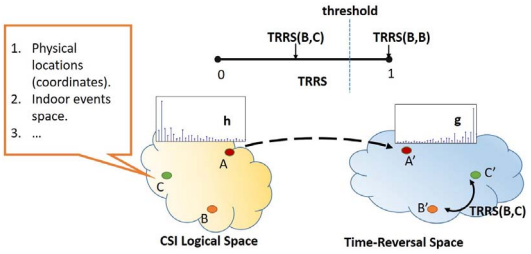

Fig. 2. Mapping between the CSI logical space and the TR space [37].

a physical locations or an indoor events in the real world, we are going to use the multipath profile to represent them directly. Moreover, the CSI obtained from WiFi devices is in the frequency domain, i.e., the CSI is in the form of the channel frequency response (CFR). In the time domain where the CSI is represented by the channel impulse response (CIR), the TR signature is the time reversed and conjugated copy of the CIR $h(t)$, i.e., $g(t) = h^*(-t)$. Hence, in the frequency domain the corresponding TR signature $\mathbf{g}$ of the CFR $\mathbf{h}$ is given by $\mathbf{g} = \mathcal{F}\{g(t)\} = \mathcal{F}\{h^*(-t)\} = \mathbf{h}^*$. With the help of the TR space, the similarity between two physical events or locations associated with different multipath profiles, also known as, CFRs, is quantified by TRRS which is defined as follows.

Definition: The TRRS $\mathcal{TR}(\mathbf{h}_1, \mathbf{h}_2)$ between two CFRs $\mathbf{h}_1$ and $\mathbf{h}_2$ is defined as

$$\mathcal{TR}(\mathbf{h}_1, \mathbf{h}_2) = \frac{\left|\sum_k g_1^*[k] g_2[k]\right|^2}{\left(\sum_{l=0}^{L-1} |g_1[l]|^2\right)\left(\sum_{l=0}^{L-1} |g_2[l]|^2\right)} = \frac{\left|\sum_k h_1[k] h_2^*[k]\right|^2}{\left(\sum_{l=0}^{L-1} |h_1[l]|^2\right)\left(\sum_{l=0}^{L-1} |h_2[l]|^2\right)} \quad (1)$$

where L is the length of the CFR vector, k is the subcarrier index, and $(\cdot)^*$ denotes taking conjugation.

The higher the TRRS is, the more similar two CFRs are. When the TRRS between two CFRs exceeds a certain value, then both of them can be viewed as representing the same physical location or indoor event. In [39] and [40], a centimeter-level accurate indoor locationing system was proposed and implemented by mapping indoor physical locations into logical locations in the TR space. TR technique has been applied to indoor passive RF sensing systems to detect indoor events and identify humans with a high accuracy [25], [37].

In this paper, by leveraging the information of indoor activities and events embedded in wireless channels, we adopt the TR technique and propose an indoor monitoring system that can detect indoor events and human motion in real time with commodity WiFi devices. Unlike the aforementioned works which use the TRRS directly, the proposed system relies on the statistics of TRRS to classify different multipath profiles, with the purpose of monitoring indoor environment. The details are discussed in the following.

B. Statistics of TRRS

Based on the assumption of channel stationarity, if CFRs $\mathbf{h}_0$ and $\mathbf{h}_1$ are captured from the same indoor multipath propagation environment, we can model $\mathbf{h}_1$ as

$$\mathbf{h}_1 = \mathbf{h}_0 + \mathbf{n} \quad (2)$$

where $\mathbf{n}$ is the Gaussian noise vector, $\mathbf{n} \sim \mathcal{CN}(\mathbf{0}, [(\sigma^2)/L]\mathbb{I})$, and $E[\|\mathbf{n}\|^2] = \sigma^2$ with $\|\cdot\|_2$ representing the $L2$-norm of a vector.

Without loss of generality, we assume unit channel gain for $\mathbf{h}_0$, i.e., $\|\mathbf{h}_0\|^2 = 1$. Then, the TRRS defined in Section II-A between $\mathbf{h}_0$ and $\mathbf{h}_1$ can be calculated as

$$\mathcal{TR}(\mathbf{h}_0, \mathbf{h}_1) = \frac{\left|\sum_k h_0^*[k](h_0[k] + n[k])\right|^2}{\|\mathbf{h}_0\|^2 \|\mathbf{h}_0 + \mathbf{n}\|^2} = \frac{\left|1 + \mathbf{h}_0^{\mathrm{H}}\mathbf{n}\right|^2}{\|\mathbf{h}_0 + \mathbf{n}\|^2} \quad (3)$$

where $(\cdot)^{\mathrm{H}}$ denotes the Hermitian operator, i.e., transpose and conjugate.

Based on (3), we introduce a new metric γ and its definition is given by the following:

$$\gamma = 1 - \mathcal{TR}(\mathbf{h}_0, \mathbf{h}_1) = 1 - \frac{\left|1 + \mathbf{h}_0^{\mathrm{H}}\mathbf{n}\right|^2}{\|\mathbf{h}_0 + \mathbf{n}\|^2} = \frac{\|\mathbf{n}\|^2 - \left|\mathbf{h}_0^{\mathrm{H}}\mathbf{n}\right|^2}{\|\mathbf{h}_0 + \mathbf{n}\|^2}. \quad (4)$$

According to the Cauchy–Schwartz inequality, we can have $|\mathbf{h}_0^{\mathrm{H}}\mathbf{n}|^2 \le \|\mathbf{n}\|^2\|\mathbf{h}_0\|^2$, with equality holds if and only if $\mathbf{n}$ is a multiplier of $\mathbf{h}_0$, which is rare to happen since $\mathbf{n}$ is a Gaussian random vector and $\mathbf{h}_0$ is deterministic. Hence, we can assume $\|\mathbf{n}\|^2 > |\mathbf{h}_0^{\mathrm{H}}\mathbf{n}|^2$ given $\|\mathbf{h}_0\|^2 = 1$, leading to $\gamma > 0$.

By taking the logarithm on both sides of (4), we have

$$\ln(\gamma) = \ln\left(\|\mathbf{n}\|^2 - \left|\mathbf{h}_0^{\mathrm{H}}\mathbf{n}\right|^2\right) - \ln\left(\|\mathbf{h}_0 + \mathbf{n}\|^2\right). \quad (5)$$

Let us denote $X = [2L/(\sigma^2)]\|\mathbf{n}\|^2$, $Y = [2L/(\sigma^2)]|\mathbf{h}_0^{\mathrm{H}}\mathbf{n}|^2$ and $Z = [2L/(\sigma^2)]\|\mathbf{h}_0 + \mathbf{n}\|^2$. It is easy to prove that $X \sim \chi^2(2L)$, $Y \sim \chi^2(2)$ and $Z \sim \chi^2_{2L}([2L/(\sigma^2)])$. Here, $\chi^2(k)$ denotes a chi-squared distribution with k degrees of freedom, and $\chi^2_k(\mu)$ represents a noncentral chi-squared distribution with k degrees of freedom and noncentrality parameter μ. By utilizing the statistics of X, Y, and Z, we can have the following properties as:

$$E\left[\|\mathbf{n}\|^2\right] = \sigma^2 \quad \mathrm{Var}\left[\|\mathbf{n}\|^2\right] = \frac{\sigma^4}{L}$$
$$E\left[|\mathbf{h}_0^{\mathrm{H}}\mathbf{n}|^2\right] = \frac{\sigma^2}{L} \quad \mathrm{Var}\left[|\mathbf{h}_0^{\mathrm{H}}\mathbf{n}|^2\right] = \frac{\sigma^4}{L^2}$$
$$E\left[\|\mathbf{h}_0 + \mathbf{n}\|^2\right] = 1 + \sigma^2 \quad \mathrm{Var}\left[\|\mathbf{h}_0 + \mathbf{n}\|^2\right] = \frac{\sigma^4 + 2\sigma^2}{L} \quad (6)$$

where $E[\,\cdot\,]$ denotes the expectation and $\mathrm{Var}[\,\cdot\,]$ represents the variance.

According to (6), it is reasonable to establish the following approximation as $|\mathbf{h}_0^{\mathrm{H}}\mathbf{n}|^2 \simeq [(\sigma^2)/L]$, whose mean square error of approximation is equal to $\mathrm{Var}[|\mathbf{h}_0^{\mathrm{H}}\mathbf{n}|^2] = [(\sigma^4)/(L^2)]$. Considering that in a typical OFDM system σ^4 usually has a magnitude smaller than 10^{-4} after normalization while L^2 is about 10^4, we have $\mathrm{Var}[|\mathbf{h}_0^{\mathrm{H}}\mathbf{n}|^2] = [(\sigma^4)/(L^2)] \to 0$. Then, substituting $|\mathbf{h}_0^{\mathrm{H}}\mathbf{n}|^2$ with $[(\sigma^2)/L]$, (5) becomes the following:

$$\ln(\gamma) \simeq \ln\left(\frac{\sigma^2}{2L}X - \frac{\sigma^2}{L}\right) - \ln\left(\frac{\sigma^2}{2L}Z\right) = \ln\left(\sigma^2\right) + \ln\left(\frac{1}{2L}X - \frac{1}{L}\right) - \ln\left(\frac{\sigma^2}{2L}Z\right). \quad (7)$$

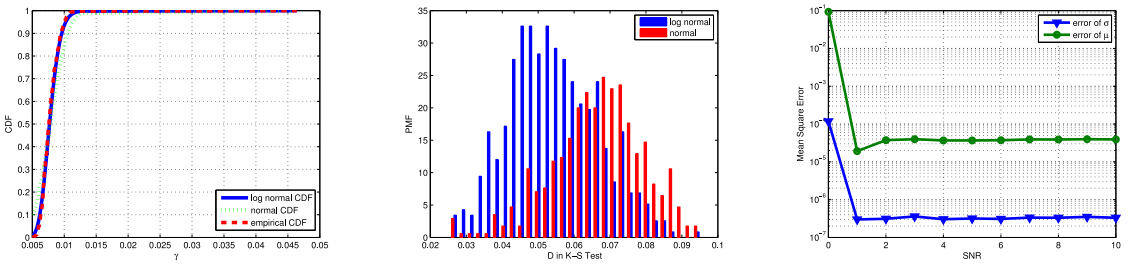

(a) (b) (c)

Fig. 3. Examples for evaluating the derived statistical model. (a) Distribution fitting for 500 real CSI measurements. (b) Histogram of scores of K–S test from 500 real CSI measurements. (c) Mean square error of log-normal parameter estimation for simulated CFRs.

Moreover, considering that it is typical to have $L > 100$ and $\sigma^2 < 10^{-2}$ in a real OFDM system, $(1/2L)X - (1/L) \to 1$ with a mean square error being $1/L^2+1/L$ which approximates to 0. Similarly, it is easy to derive that $[(\sigma^2)/2L]Z \to 1$. By utilizing the linear approximation of logarithm, i.e., $\ln(x + 1) \simeq x$ when $x \to 0$, along with $(1/2L)X - (1/L) \to 1$ and $[(\sigma^2)/2L]Z \to 1$, (7) can be approximated as follows:

$$\begin{aligned}\ln(\gamma) &\simeq \ln(\sigma^2) + \left(\frac{1}{2L}X - \frac{1}{L} - 1\right) - \left(\frac{\sigma^2}{2L}Z - 1\right) \\ &= \ln\left(\sigma^2\right) - \frac{1}{L} + \frac{1}{2L}\left(X - \sigma^2 Z\right). \end{aligned} \tag{8}$$

Referring to the definition of X and Z, the last term in (8) can be rewritten as

$$X - \sigma^2 Z = \frac{2L}{\sigma^2}\|\mathbf{n}\|^2 + 2L\|\mathbf{h}_0 + \mathbf{n}\|^2 = \sum_{i=1}^{2L} W_i$$

where W_i is defined as follows:

$$W_i = \begin{cases} w_i^2 - \left(\sqrt{2L}\Re\{h_0[k]\} + \sigma w_i\right)^2, & \text{if } i = 2k \\ w_i^2 - \left(\sqrt{2L}\Im\{h_0[k]\} + \sigma w_i\right)^2, & \text{if } i = 2k-1. \end{cases} \tag{9}$$

Here, w_i is independent and identically distributed with $w_i \sim \mathcal{N}(0, 1), \forall i$. $\Re\{\cdot\}$ denotes the function to take the real part of a complex value while $\Im\{\cdot\}$ for the imaginary part. Given the statistics of w_i, the mean and variance of W_i are derived and listed in (10) and (11), respectively

$$E[W_i] = \begin{cases} 1 - 2L\Re\{h_0[k]\}^2 - \sigma^2, & \text{if } i = 2k \\ 1 - 2L\Im\{h_0[k]\}^2 - \sigma^2, & \text{if } i = 2k-1 \end{cases} \tag{10}$$

and

$$\text{Var}\,[W_i] = \begin{cases} 2\left(1 + \sigma^4 + \left(2L\Re\{h_0[k]\}^2 - 1\right)\sigma^2\right), \\ \qquad \text{if } i = 2k \\ 2\left(1 + \sigma^4 + \left(2L\Im\{h_0[k]\}^2 - 1\right)\sigma^2\right), \\ \qquad \text{if } i = 2k-1. \end{cases} \tag{11}$$

Due to the fact that $L > 100$ in typical OFDM system, $\sum_i^{2L} W_i$ will exhibit an asymptotic behavior, according to the *central limit theorem*. Hence we define a new normal-distributed variable S_{2L} as follows:

$$S_{2L} = \frac{\sum_i^{2L} W_i + 2L\sigma^2}{\sqrt{4L\left(1 + \sigma^4\right)}} \sim \mathcal{N}(0, 1). \tag{12}$$

After substituting (12) into (9), we finally get the statistical distribution of γ as follows:

$$\begin{aligned}\ln(\gamma) &\simeq \ln\left(\sigma^2\right) - \frac{1}{L} + \frac{1}{2L}\sum_{i=1}^{2L} W_i \\ &= \ln\left(\sigma^2\right) - \frac{1}{L} - \sigma^2 + \frac{\sqrt{4L\left(1+\sigma^4\right)}}{2L} S_{2L} \\ &\sim \mathcal{N}\left(\ln\left(\sigma^2\right) - \frac{1}{L} - \sigma^2, \frac{1+\sigma^4}{L}\right). \end{aligned} \tag{13}$$

Hence, the metric γ, i.e., $1 - \mathcal{TR}(\mathbf{h}_0, \mathbf{h}_1)$, follows the log-normal distribution with the location parameter $\mu_{\text{logn}} = \ln(\sigma^2) - (1/L) - \sigma^2$ and the scale parameter $\sigma_{\text{logn}} = \sqrt{[(1 + \sigma^4)/L]}$.

The derived statistical model is verified by fitting over real measured CSI samples and CSI samples generated from the model in (2), as shown in Fig. 3. First, we adopt the Kolmogorov–Smirnov test (K–S test) to quantitatively evaluate the accuracy of the derived log-normal distribution model on the real CSI measurements. The score of K–S test is denoted as D which measures the difference between the empirical cumulative distribution function (E-CDF) and the log-normal cumulative distribution function (CDF). As depicted by the example in Fig. 3(a) and (b), the log-normal distribution fits better over CSI samples captured from real channels, compared with the normal distribution. Moreover, the derived log-normal distribution model is further investigated on simulated CSI samples through studying the mean square errors of parameter estimations against the signal-to-noise radio (SNR), also known as, σ^{-1} in dB. As plotted in Fig. 3(c), in terms of parameter estimation for the log-normal distribution, the derived model is accurate with almost zero mean square error, especially when SNR is high.

III. Design of TRIMS

Intelligent systems have become popular recently, in that with the help of learning they are capable of comprehending an object or even the world in the way humans do. For example, researchers have spent decades on computer vision or machine vision systems that achieve a high-level understanding over digital images and videos which is comparable or even better than the human visual system.

Can WiFi perceive an indoor environment? To answer this question, in this paper, we propose an intelligent indoor monitoring system, TRIMS, which enables real-time indoor monitoring with commercial WiFi devices by leveraging TR technique. This novel indoor monitoring system consists of the following components.

1) *Event Detector:* With the purpose of perceiving a monitored environment and recognizing specific events, an event detector is included in TRIMS. The proposed event detector in TRIMS relies on TR technique to evaluate the difference and similarity between various indoor events. It consists of an offline training phase where the CSI and corresponding statistics of training events are learned and an online monitoring phase where the event detector of TRIMS will report the occurrence of trained events in real time. The details are discussed in Section III-A.
2) *Motion Detector:* TRIMS not only has the functionality of detecting the occurrence of trained events, it is also capable of detecting dynamics in the environment, i.e., motion inside the protected area. The proposed motion detector leverages fluctuations in TRRS values within a time window to indicate environmental dynamics and the sensitivity is auto-adapted for each environment through the training phase. In Section III-B, we will introduce details of the proposed motion detector in TRIMS.

A. TRIMS: Event Detector

By leveraging the fundamental theories and techniques proposed in Section II, we design a real-time event detection module in TRIMS, utilizing the statistics of TRRS between the CSI as the metric for categorizing indoor environments and recognizing different indoor events. In this section, the details of statistics-based event detector are introduced, and the diagram illustrating how the event detector works is shown in Fig. 4. The details are discussed in the following.

1) Offline Training Phase: In the offline training phase, the proposed system aims to build a database that stores, for each of the training events, the log-normal statistics of TRRSs between the intraclass CSI and a representative CSI sample.

Specifically, for each indoor event $S_i \in \mathcal{S}$ with $\mathcal{S}$ being the set of indoor events to be monitored, the corresponding CFRs are obtained through channel sounding and estimated at the RX side as

$$\mathbf{H}_i = \left[\mathbf{h}_i^{(1)},\ \mathbf{h}_i^{(2)}, \ldots, \mathbf{h}_i^{(M)}\right], \quad i = 1,\ 2, \ldots, N \tag{14}$$

where N is the size of $\mathcal{S}$, i.e., the number of events of interest and M is the number of links between the TX and the RX. Each link represents the channel between a single TX–RX antenna pair. The dimension of $\mathbf{H}_i$ is $L \times M$ with L being the number of active subcarriers in a wireless OFDM system. The statistics of intraclass TRRS is estimated through the following steps.

1) *Preprocessing:* A phase sanitization algorithm is applied to compensate all CFRs for phase offsets, which are introduced by carrier frequency offset, sampling frequency offset, and symbol timing offset.

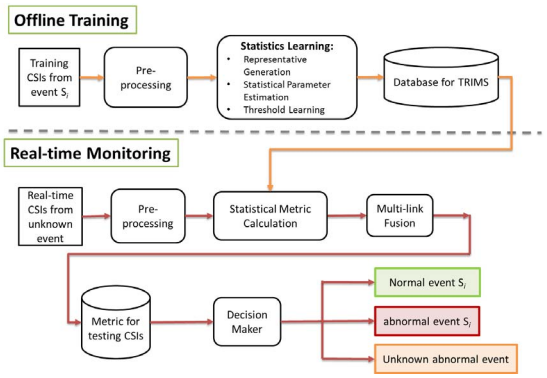

Fig. 4. Diagram of the proposed event detector in TRIMS.

2) *CSI Representative Generation:* For each link m, a CSI representative is found for every indoor event S_i in the training set. The CSI representative is selected as the one that is most similar to all other CFRs on link m from S_i. In particular, to quantitatively evaluate the similarity, the pair-wise TRRSs on link m between all the CFRs collected for indoor event S_i are calculated first. Then the CSI representative is selected on link m for event S_i as the one that is most similar to the majority of other CSI samples in the same class. $\mathbf{H}_{\text{rep},i}$ is the collection of CSI representatives on all links for event S_i, which is defined as follows:

$$\mathbf{H}_{\text{rep},i} = \left[\mathbf{h}_{\text{rep},i}^{(1)},\ \mathbf{h}_{\text{rep},i}^{(2)}, \ldots, \mathbf{h}_{\text{rep},i}^{(M)}\right] \quad \forall i. \tag{15}$$

3) *Lognormal Parameter Estimation:* Once the CSI representative is selected, the log-normal distribution parameters can be estimated from intraclass TRRSs. For link m and event S_i, the TRRSs between the CSI representative $\mathbf{h}_{\text{rep},i}^{(m)}$ and all other realizations $\mathbf{h}_i^{(m)}(n)$, $\forall\ n$ are calculated using (1) and denoted as

$$\mathcal{TR}_i^{(m)}(n) = \mathcal{TR}\left(\mathbf{h}_{\text{rep},i}^{(m)}, \mathbf{h}_i^{(m)}(n)\right) \quad n = 1, 2, \ldots, Z-1 \tag{16}$$

where n is the realization index of CFRs collected for event S_i, and Z is the total number of CFRs. Then the log-normal parameters $(\mu_i^{(m)}, \sigma_i^{(m)})$ of $\gamma = 1 - \mathcal{TR}_i^{(m)}$ for event S_i on link m are estimated by

$$\mu_i^{(m)} = \frac{1}{Z-1}\sum_{n=1}^{Z-1} \ln\left(1 - \mathcal{TR}_i^{(m)}(n)\right) \tag{17}$$

$$\sigma_i^{(m)} = \sqrt{\text{Var}\left[\ln\left(1 - \mathcal{TR}_i^{(m)}\right)\right]} \tag{18}$$

where Var[·] is the sample variance function. The training database is built with the collection of CSI representatives and log-normal distribution parameters for all the trained events. All the trained events can be divided into two groups: a) the normal events group $\mathcal{S}_{\text{normal}}$ where no alarm will be sounded when being detected and b) the abnormal events group $\mathcal{S}_{\text{abnormal}}$ where an alarm will be reported to users when an abnormal event is detected.

4) *Threshold Learning:* Based on the knowledge of $\mathcal{H}_{\text{rep}}$ and $\mathcal{Q}_{\text{rep}}$, the system builds the normal event checker and the abnormal event checker, through which the label of the testing CSI sample is determined in the monitoring phase. To determine whether event a testing CSI sample $\mathbf{H}_{\text{test}}$ belongs to an event S_i, a score is calculated first as

$$\mathcal{W}_{i,\text{test}} = \prod_{m=1}^{M} \mathcal{W}_{i,\text{test}}^{(m)} = \prod_{m=1}^{M} F_{\left(\mu_i^{(m)},\sigma_i^{(m)}\right)}\left(1 - \mathcal{TR}_{i,\text{test}}^{(m)}\right) \tag{19}$$

where $\mathcal{TR}_{i,\text{test}}^{(m)} = \mathcal{TR}(\mathbf{h}_{\text{rep},i}^{(m)}, \mathbf{h}_{\text{test}}^{(m)})$. $\mathcal{W}_{i,\text{test}}^{(m)}$ is the statistical metric on link m of $\mathbf{H}_{\text{test}}$ conditioned on event S_i, defined as the value of log-normal CDF of $1 - \mathcal{TR}_{i,\text{test}}^{(m)}$ with parameter being $\mu_i^{(m)}$ and $\sigma_i^{(m)}$. The operation $\prod_{m=1}^{M}(\cdot)$ fuses the information among all links. $F_{(\mu,\sigma)}(x)$ represents the CDF of log-normal distribution with parameters (μ, σ) and the variable x. The smaller the value of $\mathcal{W}_{i,\text{test}}^{(m)}$ is, the higher the probability for $\mathbf{H}_{\text{test}}$ belonging to event S_i is. Two thresholds γ_{normal} and γ_{abnormal} are required for the normal event checker and the abnormal event checker to define the boundary for the value of metric $\mathcal{W}_{i,j}$. Consequently, when the value of $\mathcal{W}_{i,\text{test}}$ falls below the threshold γ_{normal} or γ_{abnormal}, $\mathbf{H}_{\text{test}}$ is viewed as from event S_i. Hence, in order to correctly distinguish different events, both γ_{normal} and γ_{abnormal} are carefully learned based on the metrics $\mathcal{W}_{i,\text{test}}$ where $\mathbf{H}_{\text{test}}$ is replaced by $\mathbf{H}_{\text{rep},j}$ during the training phase. The criteria for choosing γ_{normal} and γ_{abnormal} are as follows:

$$\begin{aligned} \gamma_{\text{normal}} &= \min_{S_i \in \mathcal{S}_{\text{normal}},\ S_j \in \mathcal{S}_{\text{abnormal}}} \mathcal{W}_{i,j} \\ \gamma_{\text{abnormal}} &= \min_{S_i \in \mathcal{S}_{\text{abnormal}},\ S_j \in \mathcal{S},\ S_j \neq S_i} \mathcal{W}_{i,j}. \end{aligned} \tag{20}$$

2) Online Monitoring Phase: The statistics-based event detector is designed to identify the real-time indoor events with the knowledge of training database. Once the occurrence of a trained event is detected, the system will decide to sound an alarm based on the characteristics of that event. If an untrained event is detected, the system will also notify user about the situation. The details are discussed as follows.

During the monitoring phase, the RX keeps monitoring the environment by collecting the CSI as $\mathbf{H}_{\text{test}} = [\mathbf{h}_{\text{test}}^{(1)}, \mathbf{h}_{\text{test}}^{(2)}, \ldots, \mathbf{h}_{\text{test}}^{(M)}]$.

1) *Statistical Metric Calculation:* Since the obtained CSI measurement $\mathbf{H}_{\text{test}}$ is corrupted by random phase offsets, a phase sanitization algorithm is applied. After that, for each trained indoor event, the TRRS between the CSI representative and the testing measurement is calculated. Given the TRRSs between the testing CSI sample and trained events, the statistical metric $\mathcal{W}_{i,\text{test}}$ between $\mathbf{H}_{\text{test}}$ and the trained event S_i is calculated using (19).
2) *Decision:* The statistical metric $\mathcal{W}_{i,\text{test}}^{(m)}$ is a monotonic function of $\mathcal{TR}_{i,\text{test}}^{(m)}$ which depicts the similarity between the testing CSI samples and the CSI representative of event S_i. In other words, the more similar two CSI samples are, the smaller the value of $\mathcal{W}_{i,\text{test}}$ is. The detailed decision protocol based on $\mathcal{W}_{i,\text{test}}$ is described in the following.
   a) *Step 1 (Normal Event Checker):* To begin with, the event detector checks whether the environment is normal, i.e., only one of the normal events in S_{normal} occurs, by the following rule:

$$D_{\text{event}} = \begin{cases} \arg\ \min_{S_i \in \mathcal{S}_{\text{normal}}} \mathcal{W}_{i,\text{test}} \\ \text{if } \min_{S_i \in \mathcal{S}_{\text{normal}}} \mathcal{W}_{i,\text{test}} \leq \gamma_{\text{normal}} \\ \text{go to step 2, otherwise.} \end{cases} \tag{21}$$

   b) *Step 2 (Abnormal Event Checker):* In order to determine which trained abnormal event in S_{abnormal} occurs, it follows the rule:

$$D_{\text{event}} = \begin{cases} \arg\ \min_{S_i \in \mathcal{S}_{\text{abnormal}}} \mathcal{W}_{i,\text{test}} \\ \quad \text{if } \min_{S_i \in \mathcal{S}_{\text{abnormal}}} \mathcal{W}_{i,\text{test}} \leq \gamma_{\text{abnormal}} \\ 0, \quad \text{otherwise} \end{cases} \tag{22}$$

   where $D_{\text{event}} = 0$ indicates the occurrence of some untrained event.

To summarize, the event detector labels the CSI sample $\mathbf{H}_{\text{test}}$ by the following rule:

$$D_{\text{event}} = \begin{cases} \arg\ \min_{S_i \in \mathcal{S}_{\text{normal}}} \mathcal{W}_{i,\text{test}} \\ \quad \text{if } \min_{S_i \in \mathcal{S}_{\text{normal}}} \mathcal{W}_{i,\text{test}} \leq \gamma_{\text{normal}} \\ \arg\ \min_{S_i \in \mathcal{S}_{\text{abnormal}}} \mathcal{W}_{i,\text{test}} \\ \quad \text{if } \min_{S_i \in \mathcal{S}_{\text{normal}}} \mathcal{W}_{i,\text{test}} > \gamma_{\text{normal}} \text{ and} \\ \quad \min_{S_i \in \mathcal{S}_{\text{abnormal}}} \mathcal{W}_{i,\text{test}} \leq \gamma_{\text{abnormal}} \\ 0, \quad \text{otherwise.} \end{cases} \tag{23}$$

B. TRIMS: Motion Detector

TRIMS is designed not only to determine which trained indoor event happens, but also to detect if environment has any dynamics by means of a motion detector proposed in TRIMS.

Motion always introduces fluctuations in the radio propagation environment, leading to significant changes of TRRSs between CSI samples within a time window. The impact introduced by motion is larger compared to the impacts brought by channel fading and noise, especially when motion happens close to the TX or the RX. In this part, we propose a motion detector which uses the variance of TRRSs between CSI samples within an observation window as the metric to indicate the indoor dynamics. The proposed motion detector consists of two phases: an offline training phase and a real-time monitoring phase. The flow chart of the proposed motion detector is depicted in Fig. 5.

1) Phase I—Offline Training: In the training phase, the proposed motion detector is trained with the dynamics, measured by the variance of a TRRSs time sequence, under both static state and dynamic state with motion in the indoor environment. The detailed steps are listed as follows.

1) *Data Acquisition:* First, the state of an indoor environment is divided into two classes: a) $\mathcal{S}_1$ where the environment is static and b) $\mathcal{S}_0$ where there is some motion happening in the monitoring area. The CSI

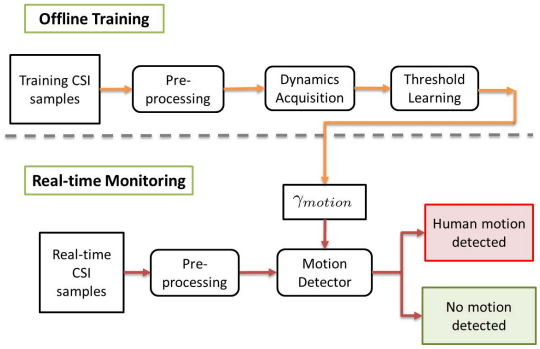

Fig. 5. Diagram of the proposed motion detector in TRIMS.

is collected continuously in time for both classes as $\mathbf{H}_i(t) = [\mathbf{h}_i^{(1)}(t), \mathbf{h}_i^{(2)}(t), \ldots, \mathbf{h}_i^{(M)}(t)]$, where $\mathbf{H}_0(t)$ is collected when the environment is static and $\mathbf{H}_1(t)$ is from the dynamic environment. t is the time instance when the CFR is captured. The phase offset in CFRs is compensated individually and independently before learning the dynamics.

2) *Dynamics Acquisition:* After time sequences of CFR measurements under both static state $\mathcal{S}_0$ and dynamic state $\mathcal{S}_1$ are obtained, the environmental dynamics is evaluated by tracking the variance of TRRSs within a time window. To study the variance under both states $\mathcal{S}_i$, $i = 0, 1$, a sliding window with length W samples and overlap $W-1$ is applied on the time sequence of $\mathbf{H}_i(t)$. For example, in a window of length W, CFRs from $\mathbf{H}_i(t_0)$ to $\mathbf{H}_i(t_0 + (W-1) * T_s)$ are stored, where T_s is the channel probing interval. Within each window, the corresponding TRRS sequence between t_0 and $t_0 + (W-1) * T_s$ is denoted as $\mathcal{TR}(\mathbf{H}_i(t_0), \mathbf{H}_i(t))$, $t_0 \leq t \leq t_0 + (W-1) * T_s$, which is calculated as follows:

$$\mathcal{TR}(\mathbf{H}_i(t_0), \mathbf{H}_i(t)) = \frac{\sum_{m=1}^{M} \mathcal{TR}\left(\mathbf{h}_i^{(m)}(t_0), \mathbf{h}_i^{(m)}(t)\right)}{M}. \tag{24}$$

Then the dynamics within the time window can be quantitatively evaluated by the variance of $\{\mathcal{TR}(\mathbf{H}_i(t_0), \mathbf{H}_i(t)), \ t_0 \leq t \leq t_0 + (W-1) * T_s\}$, which is denoted as $\sigma_i(t_0), i = 0, 1$. In order to have a fair and comprehensive analysis, multiple $\sigma_i's, i = 0, 1$ are captured at different time.

3) *Threshold Learning:* After dynamics acquisition, multiple instances of σ_0 and σ_i are obtained, and the threshold γ_{motion} for differentiating between S_0 and S_i is determined by

$$\gamma_{\text{motion}} = \begin{cases} \alpha \max_t \ \sigma_0(t) + (1-\alpha)\overline{\sigma_1(t)} \\ \qquad\qquad \text{if } \max_t \sigma_0(t) \leq \overline{\sigma_1(t)} \\ \max_t \ \sigma_0(t), \ \text{otherwise} \end{cases} \tag{25}$$

where $\overline{\sigma_1(t)}$ denotes the average of multiple $\sigma_1's$ captured at different time. α, $0 \leq \alpha \leq 1$, is a sensitivity coefficient for motion detections in that the sensitivity of the proposed motion detector increases as α decreases.

2) Phase II—Online Monitoring: During the online monitoring phase, the dynamics in the environment is tracked by comparing the variance on real-time TRRSs with γ_{motion} as

$$D_{\text{motion}}(t_0) = \begin{cases} 1, & \sigma_{\text{test}}(t_0) \geq \gamma_{\text{motion}} \\ 0, & \text{otherwise} \end{cases} \tag{26}$$

where $\sigma_{\text{test}}(t_0)$ is the variance on the testing TRRS sample sequence within a window of length W and overlap $W-1$ at time instance t_0. $D_{\text{motion}}(t_0) = 1$ indicates the existence of motion, i.e., someone is moving inside the monitoring area, while $D_{\text{motion}}(t_0) = 0$ means the environment is static.

C. TRIMS: Time-Diversity for Smoothing

In a real environment, noise in wireless transmission and outside activities exist and corrupt the estimated CSI, leading to a misdetection or a false alarm in both event detector and motion detector of TRIMS. However, by leveraging the fact that these interferences are typically sparse and abrupt, a smoothing method relying on the time diversity is proposed in this paper to address that problem.

The essential idea of the proposed time-diversity smoothing algorithm is by applying the majority vote over decisions of each testing CSI sample, assuming that the typical indoor event lasts for a couple of seconds. In both of the event detector and the motion detector, decisions will be accepted only if they are consistent along a short time period. The details are as follows.

With the help of a sliding window SW whose length is W and overlap length is O, the decisions $D_{\text{out}}(n)$ at time index n is obtained through

$$D_{\text{out}}(w) = \text{MV}\{D_{\text{in}}(1 + (w-1) * O), \ldots, D_{\text{in}}(W + (w-1) * O)\} \tag{27}$$

where $D_{\text{in}}(w)$ is the input decision sample at time index w and $\text{MV}\{\cdot\}$ is the operator for taking majority vote. The corresponding time delay introduced by the sliding window SW is in general $(W-O) \times T$, where T is the time interval between consecutive D_{in} samples.

For example, in order to alleviate false alarms introduced by outside activities and imperfect CSI estimation to the proposed event detector, a two-level time-diversity smoothing is applied as follows.

1) *Level I:* A majority vote is applied directly on the raw decisions D_{motion} of each single CSI sample. Given a sliding window SW_1 whose length is W_1 and overlap length is O_1, the decisions of index w, $D_{\text{MV1}}(w)$, is obtained from taking a majority vote over $D_{\text{event}}(i + (w-1) * O_1)$, $1 \leq i \leq W_1$.
2) *Level II:* A second sliding window SW_2 is applied on $D_{\text{MV1}}(w)$ with length W_2 and overlap O_2. Consequently, the final decision output is $D_{\text{final}}(n)$. The system suffers a time delay $(W_2 - O_2) \times (W_1 - O_1) \times T_s$.

IV. Experimental Results

In order to evaluate the feasibility and the performance of the proposed TRIMS in indoor monitoring, we build a prototype on commodity WiFi devices performing 3×3 multiple-input and multiple-output transmission at 5.845-GHz

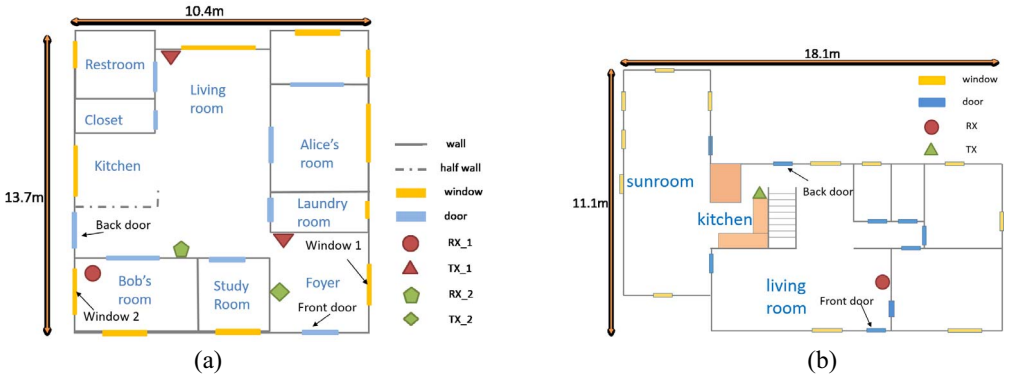

Fig. 6. Experimental setting for TRIMS. Floorplan of (a) house #1 and (b) house #2.

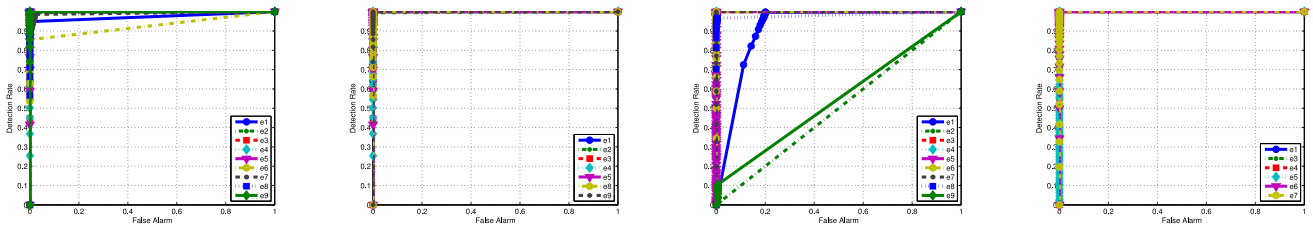

Fig. 7. ROC performance for the proposed event detector. ROC performance for (a) all events (TX in the foyer), (b) targets events (TX in the foyer), (c) all events (TX outside the study room), and (d) targets events (TX outside the study room).

carrier frequency under the IEEE 802.11n standard. According to the IEEE 802.11n standard, both 2.4-GHz band and 5-GHz band support a 40-MHz bandwidth and the CSI at those two bands should share the same resolution. Therefore, with the obtained CSI, the proposed system should achieve a detection performance at 2.4 GHz similar to that from 5.8 GHz. In the prototype, the CSI is extracted from the Qualcomm network interface card and composed by a complex-valued matrix for accessible subcarriers on all nine links. With a single pair of devices, we conduct extensive experiments in two real indoor environments: Houses #1 and #2 with regular residence activities, whose floorplans are shown in Fig. 6(a) and (b). The locations of the TX and the RX are marked in the floorplans.

TABLE I
EVENTS OF INTEREST IN HOUSE #1

State Index	Description
e1	All doors are closed.
e2	Front door open.
e3	Back door open.
e4	Bob's room door open.
e5	Study room door open.
e6	Alice's room door open.
e7	Restroom door open.
e8	Window 1 open.
e9	Window 2 open.

A. TRIMS: Event Detector

We start from the performance study of the proposed event detector in TRIMS and experiments are conducted in both facilities. In order to learn the statistics of intraclass TRRS, at least 300 realizations of CFRs corresponding to each indoor propagation environment should be collected. Furthermore, the CSI sounding rate is 100 Hz in the training phase, while it becomes 30 Hz in the real-time monitoring phase for the event detector in TRIMS. The two-level time diversity algorithm is applied in the event detector with $W_1 = 15, O_1 = 14, W_2 = 45$, and $O_2 = 15$, considering that 30 CSI samples are collected per second.

1) Study on Location of TX–RX: As discussed in the previous sections, the proposed event detector is aimed at monitoring and detecting indoor events by leveraging the TR technique to capture changes in the CSI. Different events introduce different changes, depending on not only the characteristics of each indoor event but also the distance between the event location to the transceivers. The closer the indoor event is, the larger impact it introduces. Hence, it is crucial to study how the locations of the TX and the RX affects the performance of the proposed event detector.

In house #1, we study the impact of TX–RX locations on TRIMS's performance in the event detection and the events of interest are listed in Table I, while the candidate locations of TX and RX are labeled with "TX_1" and "RX_1" in Fig. 6(a). The RX is fixed in the study room while the TX is located either in the foyer against a wall or outside the restroom. The performance is evaluated through the RX operating characteristic (ROC) curve, where the x-axis is the false alarm rate of an event e_i, i.e., the probability of other events being misclassified as e_i, whereas the y-axis is the detection rate of e_i.

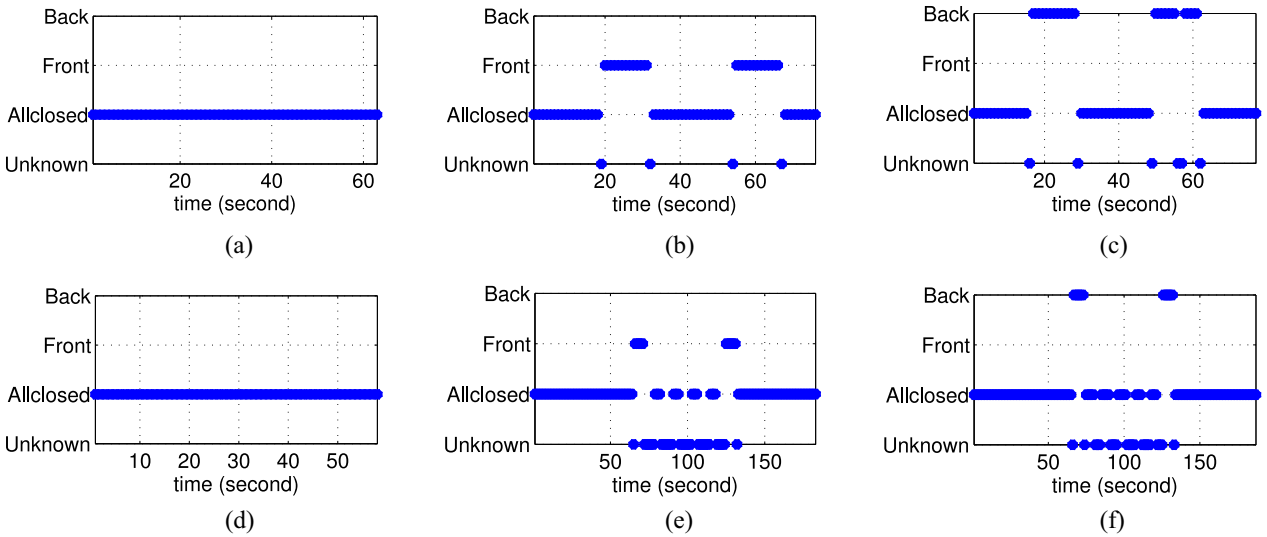

Fig. 8. Monitoring results of the proposed event detector for operational tests in house #1. Test under (a) all doors closed, (b) opening (around the 20th and the 50th s) and closing (around the 30th and the 60th s) front door from the outside the house twice, and (c) opening (around the 25th and the 55th s) and closing (around the 35th and the 65th s) back door from the outside the house twice. (d) Postman test with someone walking outside the front door. Test when an intruder (e) comes in (around the 60th s), walks inside, and leaves (around the 120th s) through front door and (f) comes in (around the 60th s), walks inside, and leaves (around the 120th s) through back door.

As shown in Fig. 7(a), the proposed event detector fails to differentiate between the CSI of e1, e6, and e7, in that the false alarm rates of e1, e6, and e7 are extremely high under the same detection rate, compared with others. The reason is that the changes in the wireless multipath channel introduced by e6 and e7 are too small for the proposed event detector to capture. A possible reason is that event e6 and e7 are far from the TX and the RX, when both devices are located in the front part of the house. Similarly, in Fig. 7(c), when the TX is put outside the study room, i.e., in the back part of the house, event e2 and e8 are too far away while e9 is outside the circle range defined by the line segment between the TX and the RX. Consequently, the proposed event detector has an ambiguity over e1, e2, e8, and e9.

Here, we introduce the concept of "target event," to whom the proposed event detector has a perfect accuracy, as shown in Fig. 7(b) and (d). The target events are those events that satisfy a rule-of-thumb, which says that in order to have it detected, the event should either be close to the TX–RX link or have a LOS path to one of the devices, given the location of the TX and the RX. Under the rule-of-thumb, the target event is able to change the CSI between the TX and the RX in a way that is significant enough. The proposed event detector can achieve a perfect ROC performance for target events.

2) Operational Test in House #1: In this part, to further study the performance of TRIMS in the real-time event monitoring, we imitate several intrusion and postman cases with locations of TX and RX being "TX_2" and "RX_2." In the intrusion test, an intruder enters the house from a door and walks inside the house before leaving from the same door. On the other hand, in the postman test, some one is walking outside the front door of each house to imitate a postman.

Moreover, in this part, the system is only trained for events e1–e3. In Fig. 8, the system output is plotted along the time. The y-axis is the output decision, where "allclosed" indicates e1, "front" and "back" represent e2 and e3, respectively, and "unknown" means untrained events happening. Take Fig. 8(a) as an example. The proposed event detector outputs state 1, i.e., "all doors are closed," during the test. As shown in Fig. 8(b), during the test, the proposed event detector first reports e1 for about 20 s and then detects the occurrence of e2 when the front door is opened at the time index of the 20th s, with a single detection over the untrained event, i.e., the output falls to unknown. The system starts to report e1 when the front door is closed at around the 30th s.

Fig. 8(a)–(c) illustrates the ability of the proposed event detector to perfectly monitor and detect the trained events in real time when: 1) the environment is quiet and all doors are closed; 2) the front door is opened and then closed twice from the outside; and 3) the back door is opened and closed twice from the outside. In Fig. 8(d), we simulate the postman case where someone wanders outside the front door, close to the target event. The proposed event detector shows its robustness to outside activities by reporting no false alarms in the postman case. In the next test, we simulate intrusions made by an intruder through the front door and the back door and the intruder is required to leave through the same door after walking inside the house for a certain period. As demonstrated in Fig. 8(e) and (f), the proposed event detector succeeds in capturing the intrusion. Moreover, between the door opening in both figures, the decision of the proposed event detector may become unknown which is owing to the interference to the multipath channel brought by human motion inside the house.

3) Long-Term Test in House #1: Furthermore, we conduct a long-term monitoring test for the proposed event detector in TRIMS in house #1 for six days. The result is compared with that of a commercial home security system whose contact sensors are installed on the front and back door. During the first six days, TRIMS has zero false alarm when the ground truth state of the indoor environment is e1. It detects with 100%

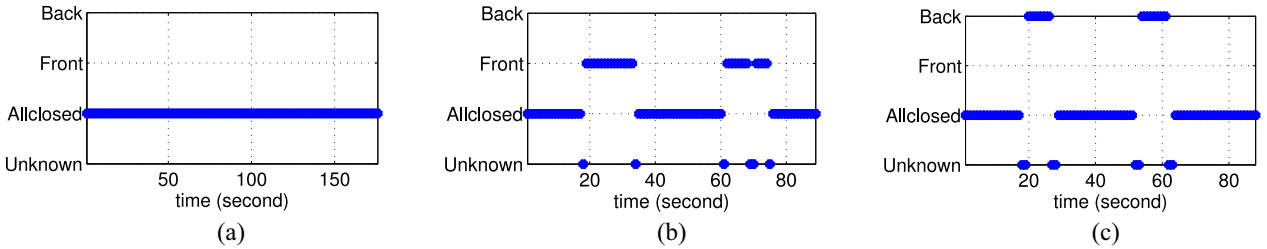

Fig. 9. Monitoring results of the proposed event detector for operational tests in house #2. Test under (a) all doors closed, (b) opening (around the 19th and the 61st s) and closing (around the 36th and the 72nd s) front door from the outside the house twice, and (c) opening (around the 18th and the 50th s) and closing (around the 28th and the 64th s) back door from the outside the house twice.

TABLE II
EVENTS OF INTEREST IN HOUSE #2

State Index	Description
e1	All doors are closed.
e2	Front door open.
e3	Back door open.

accuracy over 21 times of front door opening while detects 15 out of 18 times of back door opening, i.e., an average accuracy of 92.31%.

The degradation in the accuracy is because the wireless channel keeps fading along the time while the training data for front door opening and back door opening is not updated. Hence, there eventually will be a mismatch between the testing CSI measurements and the training profiles. Considering the channel fading, the proposed event detector is designed to have an automatic updating scheme for e1, i.e., it will periodically update the training data of e1 as long as the environment is recognized as in the state of all doors closed by the event detector. The periodic refresh of e1 training metrics is to address the uncontrollable changes in the indoor environment but fails to fully resolve the problem. Due to the difficulty of labeling the testing CSI measurements from door opening in an unsupervised way, in this paper we do not consider to update the training data for other events automatically.

4) Operational Test in House #2: In this part, the performance of TRIMS in real-time event monitoring is studied in house #2 with the event list being in Table II. Moreover, all the parameters and hardware settings are as the same as the ones in house #1.

To begin with, the proposed event detector is set to monitor when: 1) the environment is quiet and all doors are closed; 2) someone opens the front door and then closes it from the outside (twice); and 3) someone opens the back door and then closes it from the outside (twice). The results are shown in Fig. 9, where the decision output being unknown means that an untrained event is happening, allclosed indicates that environment is in the all-doors-closed and quiet, and front and back represent front door and back door is opening, respectively. All figures can be interpreted in the same way as those in Fig. 8. The proposed event detector succeeds in capturing the trained events perfectly without false alarms.

5) Long-Term Test in House #2: Furthermore, the long-term behavior of the proposed event detector in TRIMS is investigated in house #2 through a test that lasts for two weeks. During the long-term test, resident activities are more often than that in house #1 and thus the indoor environment changes every day which might jeopardize the proposed event detector trained in day 1. Every day during the long-term test, tester performed the same operational test as in Section IV-A4 to evaluate the detection performance of the proposed event detector. The system outputs along the time are plotted in Fig. 10, where y-axis is the system output with unknown, allclosed, front, and back representing the occurrence of untrained events, e1 all doors are closed, e2 "front door is opened," and e3 "back door is opened," respectively.

As shown in Fig. 10(a), (f), and (k), the proposed event detector is good at detecting the trained events with no false alarm during the same day when the system is trained. However, after one week or even two weeks, with the original training database built on day 1, the proposed system fails to detect the trained events and has a high false alarm rate on e2, as shown in Fig. 10(b), (d), (g), (i), (l), and (n). For example, as depicted in Fig. 10(b), the system keeps reporting front door is opened, when the ground truth of the indoor state being e1 all doors are closed. With uncontrolled resident activities, the indoor environment changes resulting in a different multipath profile not only for e1 but also for e2 and e3. With the help of the auto-update of e1, the proposed event detector is able to detect the trained events e2 and e3 during the two-week experiment with no false alarm. The results are as shown in Fig. 10(c), (e), (h), (j), (m), and (o).

As demonstrated by examples in Fig. 10, with an automatic and periodic update of the training data for e1, TRIMS can maintain its accuracy in differentiating between and recognizing trained events in a single family house with normal resident activities during two weeks. The monitoring results of TRIMS in the 14-day experiment is compared with the history log provided by a commercial home security system. In general, the proposed event detector captures the incidents of e2 and e3, i.e., opening the front or the back door from the outside of the house, with an accuracy being 95.45% while a single misdetection happens on day 13.

B. TRIMS: Motion Detector

The performance of the motion detector is tested in house #1 with the TX and RX devices located at positions marked by TX_2 and RX_2 in Fig. 6(a). The parameter α defined in (25)

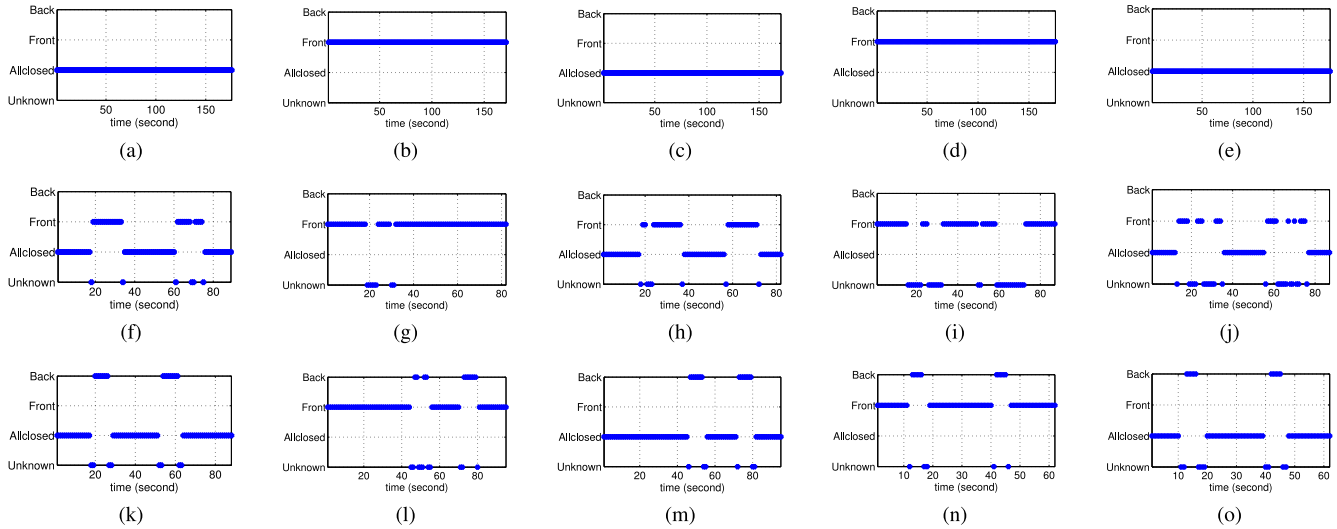

Fig. 10. Monitoring results of the event detector for long-term tests in house #2. e1 test on (a) day 1, (b) day 7 w/o e1 update, (c) day 7 w/ e1 update, (d) day 14 w/o e1 update, and (e) day 14 w/ e1 update. e2 test on (f) day 1 (open around the 20th and the 62nd s and close around the 34th and the 74th s), (g) day 7 w/o e1 update (open around the 20th and the 60th s and close around the 30th and the 70th s), (h) day 7 w/ e1 update, (i) day 14 w/o e1 update (open around the 18th and the 58th s and close around the 30th and the 70th s), and (j) day 14 w/ e1 update. e3 test on (k) day 1 (open around the 18th and the 52nd s and close around the 24th and the 62nd s), (l) day 7 w/o e1 update (open around the 46th and the 72nd s and close around the 52nd and the 80th s), (m) day 7 w/ e1 update, (n) day 14 w/o e1 update (open around the 12th and the 40th s and close around the 20th and the 48th s), and (o) day 14 w/ e1 update.

TABLE III
DETECTION RATE FOR MOTION AT DIFFERENT LOCATIONS UNDER ZERO FALSE ALARM RATE

Walking Location	**Detection Rate** $\alpha = 0.8$	**Detection Rate** $\alpha = 0.2$
Postman	0%	0%
Foyer	59.18%	12.24%
Laundry Room	100%	81.25%
Alice's Room	3.92%	0%
Study Room	1.92%	0%
Center of the house	83.33%	75.93%
Kitchen	48%	36%
Living Room	30.91%	0%
Restroom	0%	0%

is set to be either 0.8 or 0.2, while $W = 30$ indicates a 1-s window of continuously collected CSI as defined in (24). For the $D_{\text{motion}}(t_0)$ in (26), we apply a time-diversity smoothing with only one-level majority vote whose $W = 45$ and $O = 15$, to eliminate any possible false alarms due to burst noise or error in the CSI estimation.

During the training phase, the proposed motion detector learns the threshold γ_{motion} based on the data from 1-min monitoring data collected under e1, and someone walking in and around the center of the house.

Given a zero false alarm, the detection rates of motion at different locations are listed in Table III. The proposed motion detector is intelligent in that it learns and adapts its sensitivity automatically based on the characteristics of the radio propagation environment where it is deployed, through the training phase. The change that motion introduces to the channel is proportional to the amount of the reflected signal energy that is generated by the moving object and collected at the RX. Hence, by relying on the motion detector, TRIMS succeeds in captures motion inside the house occurring close to the devices or have a LOS path to either the TX or the RX. However, due to the large path loss for EM waves penetrating multiple walls, motion occurring inside the Alice's room or restroom will have no or tiny impacts on the CSI measurements and thus cannot trigger the motion detector. Moreover, a smaller value of α indicates the system being less sensitive and a smaller coverage of monitoring area.

V. DISCUSSION

In this section, we are going to discuss some limitations of TRIMS proposed in this paper, along with topics for further extending this paper.

A. Retrain of TRIMS

As discussed in the long-term test in Section IV-A3, the system keeps automatically and periodically updating the training data of e1, i.e., the state of that all doors are closed, based on its real-time detection results. Due to the difficulty in labeling the testing CSI of door opening in an unsupervised way, the proposed auto-updating scheme can only work for e1. As verified by experiments, with that automatic updating scheme, the proposed system is robust to normal EM perturbations introduced by noise and slight environmental changes. However, environmental changes affect not only the CSI of state e1, but also that of event e2 and e3. If the environment changes significantly from that when e2 and e3 were trained, the proposed system would fail to find a match between the testing CSI and the one in the training database. That is when

the system needs retraining, and it can be determined by comparing the very first e1 training data with the current one. Through experiments we found that when the TRRS between the earliest e1 training CSI and the current CSI measured under e1 drops below an empirical threshold of 0.7, the proposed system requires retraining over all states.

B. Monitoring With Multiple Transmitters

In current days, there are more than one device that usually connects to the same WiFi router in an office or at home, which inspires us to extend this paper by developing TRIMS to accommodate more TXs. The performance of TRIMS can be improved since the information has more degrees of freedom by means of an increased spatial (device-level) diversity. Moreover, as shown in Sections IV-A1 and IV-B, for a single pair of the TX and the RX devices, it has a limited coverage in detecting events and motion. By deploying more TXs at different locations, the monitoring area will be expanded. However, it requires further study to optimize the performance of the multi-TX TRIMS and will be one of our future work.

C. Detecting Dynamic Event

In the current event detector of TRIMS, the training database is built upon static CSI measurements collected for each events. Each dynamic event can be decomposed into several intermediate states sampled during its occurrence. Since the intermediate state can be viewed as static, the proposed algorithm can be applied to detect the occurrence of its intermediate states. Consequently, the state transition that depicts the occurrence of dynamic events can be captured, and thus dynamic events can also be monitored by the proposed system. Moreover, the authors are working on a new method for monitoring indoor dynamic events and details will be discussed in a future paper.

D. Identifying Motion

In this paper, the proposed motion detector in TRIMS manage to detect the incidents of motion. Nevertheless, it is worthwhile to study how to utilize the TR technique to extract the characteristics of a motion with WiFi signals, e.g., the direction and the velocity. The potentiality of extracting motion information and even identifying motion with commercial WiFi devices is beneficial to various applications like elderly assistance and life monitoring.

E. Potential of TRIMS

The proposed TRIMS is not confined by WiFi and can be applied to other wireless technologies as long as CSI with enough resolution can be obtained. The spatial resolution of CSI is determined by the transmission bandwidth of the radio frequency (RF) device. Ultrawideband (UWB) communication whose bandwidth exceeds 500 MHz can provide CSI of a finer spatial resolution and enable a better discrimination than WiFi does. However, UWB-based indoor monitoring systems require to deploy specially designed RF devices and the coverage is small. On the other hand, as demonstrated by experiments in this paper, with the help of TRIMS, commercial WiFi devices with only a 40-MHz bandwidth can support high-accuracy indoor monitoring. Due to the explosive popularity of wireless devices, increasing wireless traffic clogs WiFi and collisions delay the CSI probing with an unknown offset, which introduces difficulty to real-time wireless sensing systems. Taking advantage of the proposed smoothing algorithm, TRIMS is robust to nonuniform CSI probing and packages loss. Moreover, thanks to the ubiquitous deployment of WiFi, the proposed system is ready and can be easily put into practice for smart home indoor monitoring. In general, the proposed system can be integrated with all kinds of wireless technologies where CSI with enough resolution is accessible.

VI. Conclusion

In this paper, we present a smart radio system, TRIMS, for real-time indoor monitoring, which utilizes TR technique to exploit the information in multipath propagations. Moreover, the statistical behavior of intraclass TRRS is analyzed theoretically. An event detector is built, where different indoor events are differentiated and quantitatively evaluated through TRRS statistics of the associated CSI. Furthermore, a motion detector is designed in TRIMS to detect the existence of dynamics in the environment. The performance of TRIMS is studied through extensive experiments, which are conducted with TRIMS's prototype implemented on a single pair of commodity WiFi devices. Experimental results demonstrate that TRIMS addresses the problem of recognizing different indoor events in real-time. We also evaluate the performance through a two-week monitoring test in a single family house with normal resident activities. TRIMS succeeds in achieving a high accuracy in long-term indoor monitoring experiments, demonstrating its prominent and promising role in future intelligent WiFi-based low-complexity smart radios.

References

[1] D. Zhang, J. Ma, Q. Chen, and L. M. Ni, "An RF-based system for tracking transceiver-free objects," in *Proc. 5th Annu. IEEE Int. Conf. Pervasive Comput. Commun. (PerCom)*, Mar. 2007, pp. 135–144.

[2] S. Sigg, S. Shi, F. Buesching, Y. Ji, and L. Wolf, "Leveraging RF-channel fluctuation for activity recognition: Active and passive systems, continuous and RSSI-based signal features," in *Proc. Int. Conf. Adv. Mobile Comput. Multimedia (MoMM)*, 2013, pp. 43–52.

[3] C. Han, K. Wu, Y. Wang, and L. M. Ni, "WiFall: Device-free fall detection by wireless networks," in *Proc. Int. Conf. Comput. Commun.*, Apr. 2014, pp. 271–279.

[4] Y. Gu, F. Ren, and J. Li, "PAWS: Passive human activity recognition based on WiFi ambient signals," *IEEE Internet Things J.*, vol. 3, no. 5, pp. 796–805, Oct. 2016.

[5] H. Abdelnasser, M. Youssef, and K. A. Harras, "WiGest: A ubiquitous WiFi-based gesture recognition system," in *Proc. IEEE Conf. Comput. Commun. (INFOCOM)*, Apr. 2015, pp. 1472–1480.

[6] F. Adib and D. Katabi, "See through walls with WiFi!" in *Proc. ACM SIGCOMM Conf. (SIGCOMM)*, 2013, pp. 75–86.

[7] K. Qian, C. Wu, Z. Yang, Y. Liu, and Z. Zhou, "PADS: Passive detection of moving targets with dynamic speed using PHY layer information," in *Proc. 20th IEEE Int. Conf. Parallel Distrib. Syst. (ICPADS)*, Dec. 2014, pp. 1–8.

[8] Y. Zeng, P. H. Pathak, C. Xu, and P. Mohapatra, "Your AP knows how you move: Fine-grained device motion recognition through WiFi," in *Proc. 1st ACM Workshop Hot Topics Wireless*, 2014, pp. 49–54.

[9] A. Banerjee, D. Maas, M. Bocca, N. Patwari, and S. Kasera, "Violating privacy through walls by passive monitoring of radio windows," in *Proc. ACM Conf. Security Privacy Wireless Mobile Netw. (WiSec)*, Oxford, U.K., 2014, pp. 69–80.
[10] Y. Wang *et al.*, "E-eyes: Device-free location-oriented activity identification using fine-grained WiFi signatures," in *Proc. 20th Annu. Int. Conf. Mobile Comput. Netw.*, 2014, pp. 617–628.
[11] C. Wu *et al.*, "Non-invasive detection of moving and stationary human with WiFi," *IEEE J. Sel. Areas Commun.*, vol. 33, no. 11, pp. 2329–2342, Nov. 2015.
[12] D. Zhang, H. Wang, Y. Wang, and J. Ma, "Anti-fall: A non-intrusive and real-time fall detector leveraging CSI from commodity WiFi devices," in *Proc. Int. Conf. Smart Homes Health Telematics*, 2015, pp. 181–193.
[13] W. Wang, A. X. Liu, M. Shahzad, K. Ling, and S. Lu, "Understanding and modeling of WiFi signal based human activity recognition," in *Proc. 21st Annu. Int. Conf. Mobile Comput. Netw.*, 2015, pp. 65–76.
[14] M. A. A. Al-Qaness, F. Li, X. Ma, and G. Liu, "Device-free home intruder detection and alarm system using Wi-Fi channel state information," *Int. J. Future Comput. Commun.*, vol. 5, no. 4, p. 180, 2016.
[15] H. Wang *et al.*, "RT-FALL: A real-time and contactless fall detection system with commodity WiFi devices," *IEEE Trans. Mobile Comput.*, vol. 16, no. 2, pp. 511–526, Feb. 2017.
[16] R. Nandakumar, B. Kellogg, and S. Gollakota, "Wi-Fi gesture recognition on existing devices," *CoRR*, vol. abs/1411.5394, 2014. [Online]. Available: http://arxiv.org/abs/1411.5394
[17] K. Ali, A. X. Liu, W. Wang, and M. Shahzad, "Keystroke recognition using WiFi signals," in *Proc. 21st Annu. Int. Conf. Mobile Comput. Netw.*, 2015, pp. 90–102.
[18] R. M. Narayanan, "Through-wall radar imaging using UWB noise waveforms," *J. Frankl. Inst.*, vol. 345, no. 6, pp. 659–678, 2008.
[19] G. K. Nanani and M. Kantipudi, "A study of Wi-Fi based system for moving object detection through the wall," *Int. J. Comput. Appl.*, vol. 79, no. 7, pp. 15–18, 2013.
[20] D. Huang, R. Nandakumar, and S. Gollakota, "Feasibility and limits of Wi-Fi imaging," in *Proc. 12th ACM Conf. Embedded Netw. Sensor Syst.*, 2014, pp. 266–279.
[21] D. Pastina, F. Colone, T. Martelli, and P. Falcone, "Parasitic exploitation of Wi-Fi signals for indoor radar surveillance," *IEEE Trans. Veh. Technol.*, vol. 64, no. 4, pp. 1401–1415, Apr. 2015.
[22] F. Adib, Z. Kabelac, D. Katabi, and R. C. Miller, "3D tracking via body radio reflections," in *Proc. 11th USENIX Symp. Netw. Syst. Design Implement.*, Seattle, WA, USA, Apr. 2014, pp. 317–329.
[23] F. Adib, C.-Y. Hsu, H. Mao, D. Katabi, and F. Durand, "Capturing the human figure through a wall," *ACM Trans. Graph.*, vol. 34, no. 6, pp. 1–13, Nov. 2015.
[24] F. Adib, Z. Kabelac, and D. Katabi, "Multi-person localization via RF body reflections," in *Proc. 12th USENIX Symp. Netw. Syst. Design Implement.*, Oakland, CA, USA, May 2015, pp. 279–292.
[25] Q. Xu, Y. Chen, B. Wang, and K. J. R. Liu, "TRIEDS: Wireless events detection through the wall," *IEEE Internet Things J.*, vol. 4, no. 3, pp. 723–735, Jun. 2017.
[26] B. Bogert, "Demonstration of delay distortion correction by time-reversal techniques," *IRE Trans. Commun. Syst.*, vol. 5, no. 3, pp. 2–7, Dec. 1957.
[27] M. Fink, C. Prada, F. Wu, and D. Cassereau, "Self focusing in inhomogeneous media with time reversal acoustic mirrors," in *Proc. IEEE Ultrason. Symp.*, 1989, pp. 681–686.
[28] M. Fink, "Time reversal of ultrasonic fields. I. Basic principles," *IEEE Trans. Ultrason., Ferroelectr., Freq. Control*, vol. 39, no. 5, pp. 555–566, Sep. 1992.
[29] F. Wu, J.-L. Thomas, and M. Fink, "Time reversal of ultrasonic fields. II. Experimental results," *IEEE Trans. Ultrason., Ferroelectr., Freq. Control*, vol. 39, no. 5, pp. 567–578, Sep. 1992.
[30] B. E. Henty and D. D. Stancil, "Multipath-enabled super-resolution for RF and microwave communication using phase-conjugate arrays," *Phys. Rev. Lett.*, vol. 93, no. 24, 2004, Art. no. 243904.
[31] G. Lerosey *et al.*, "Time reversal of electromagnetic waves," *Phys. Rev. Lett.*, vol. 92, no. 19, 2004, Art. no. 193904.
[32] G. Lerosey *et al.*, "Time reversal of electromagnetic waves and telecommunication," *Radio Sci.*, vol. 40, no. 6, pp. 1–10, 2005.
[33] G. Lerosey, J. De Rosny, A. Tourin, A. Derode, and M. Fink, "Time reversal of wideband microwaves," *Appl. Phys. Lett.*, vol. 88, no. 15, 2006, Art. no. 154101.
[34] J. de Rosny, G. Lerosey, and M. Fink, "Theory of electromagnetic time-reversal mirrors," *IEEE Trans. Antennas Propag.*, vol. 58, no. 10, pp. 3139–3149, Oct. 2010.
[35] B. Wang, Y. Wu, F. Han, Y.-H. Yang, and K. J. R. Liu, "Green wireless communications: A time-reversal paradigm," *IEEE J. Sel. Areas Commun.*, vol. 29, no. 8, pp. 1698–1710, Sep. 2011.
[36] C. Chen, Y. Han, Y. Chen, and K. J. R. Liu, "Indoor global positioning system with centimeter accuracy using Wi-Fi [applications corner]," *IEEE Signal Process. Mag.*, vol. 33, no. 6, pp. 128–134, Nov. 2016.
[37] Q. Xu, Y. Chen, B. Wang, and K. J. R. Liu, "Radio biometrics: Human recognition through a wall," *IEEE Trans. Inf. Forensics Security*, vol. 12, no. 5, pp. 1141–1155, May 2017.
[38] C. Chen, Y. Han, Y. Chen, and K. J. R. Liu, "Multi-person breathing rate estimation using time-reversal on WiFi platforms," in *Proc. IEEE Glob. Conf. Signal Inf. Process.*, Dec. 2016, pp. 1059–1063.
[39] Z.-H. Wu, Y. Han, Y. Chen, and K. J. R. Liu, "A time-reversal paradigm for indoor positioning system," *IEEE Trans. Veh. Technol.*, vol. 64, no. 4, pp. 1331–1339, Apr. 2015.
[40] C. Chen, Y. Chen, H.-Q. Lai, Y. Han, and K. J. R. Liu, "High accuracy indoor localization: A WiFi-based approach," in *Proc. IEEE Int. Conf. Acoust. Speech Signal Process. (ICASSP)*, Mar. 2016, pp. 6245–6249.

Qinyi Xu (S'15) received the B.S. degree (Highest Hons.) in information engineering from Southeast University, Nanjing, China, in 2013. She is currently pursuing the Ph.D. degree at the Department of Electrical and Computer Engineering, University of Maryland at College Park, College Park, MD, USA.

She was an exchange student with the KTH Royal Institute of Technology, Stockholm, Sweden, from 2012 to 2013, with the national sponsorship of China. Her current research interests include signal processing and wireless communications.

Ms. Xu was a recipient of the Clark School Distinguished Graduate Fellowships from the University of Maryland at College Park and the Graduate with Honor Award from Southeast University in 2013.

Zoltan Safar received the University Diploma degree in electrical engineering from the Technical University of Budapest, Budapest, Hungary, in 1996, and the M.S. and Ph.D. degrees in electrical and computer engineering from the University of Maryland at College Park, College Park, MD, USA, in 2001 and 2003, respectively.

He was an Assistant Professor with the Department of Innovation, IT University of Copenhagen, Copenhagen, Denmark, until 2005. He then joined Nokia, Copenhagen, where he was a Senior Engineer of 3GPP Long Term Evolution Receiver Algorithm Design. Since 2007, he has been a Senior Engineer with Samsung Electro-Mechanics, Atlanta, GA, USA, developing physical-layer signal processing algorithms for next-generation wireless communication systems. In 2010, he became a Senior Software Engineer with Bloomberg L.P., New York, NY, USA, and he designed and implemented software systems for monitoring, configuration, and maintenance of the company's private communication network. Since 2010, he has been with the Department of Electrical and Computer Engineering, University of Maryland at College Park, where he is the Director of the MS in Telecommunications Program.

Dr. Safar was a recipient of the Outstanding Systems Engineering Graduate Student Award from the Institute for Systems Research, University of Maryland in 2003 and the Invention of the Year Award (together with W. Su and K. J. R. Liu) from the University of Maryland at College Park in 2004.

Yi Han received the B.S. degree in electrical engineering (Highest Hons.) from Zhejiang University, Hangzhou, China, in 2011, and the Ph.D. degree from the Department of Electrical and Computer Engineering, University of Maryland at College Park, College Park, MD, USA, in 2016.

He is currently the Wireless Architect of Origin Wireless, Inc., Greenbelt, MD, USA. His current research interests include wireless communication and signal processing.

Dr. Han was a recipient of the Class A Scholarship from Chu Kochen Honors College, Zhejiang University in 2008 and the Best Student Paper Award of the IEEE ICASSP in 2016.

Beibei Wang (SM'15) received the B.S. degree (Highest Hons.) from the University of Science and Technology of China, Hefei, China, in 2004, and the Ph.D. degree from the University of Maryland at College Park, College Park, MD, USA, in 2009, both in electrical engineering.

She was a Research Associate with the University of Maryland from 2009 to 2010, and Qualcomm Research and Development, San Diego, CA, USA, from 2010 to 2014. Since 2015, she has been with Origin Wireless, Inc., Greenbelt, MD, USA, where she is currently the Chief Scientist. She co-authored *Cognitive Radio Networking and Security: A Game-Theoretic View* (Cambridge Univ. Press, 2010). Her current research interests include wireless communications and signal processing.

Dr. Wang was a recipient of the Graduate School Fellowship, the Future Faculty Fellowship, and the Dean's Doctoral Research Award from the University of Maryland at College Park and the Overview Paper Award from the IEEE Signal Processing Society in 2015.

K. J. Ray Liu (F'03) was named a Distinguished Scholar–Teacher of the University of Maryland at College Park, College Park, MD, USA, in 2007, where he is a Christine Kim Eminent Professor of Information Technology. He leads the Maryland Signals and Information Group conducting research encompassing broad areas of information and communications technology with recent focus on smart radios for smart life.

Dr. Liu was a recipient of the 2016 IEEE Leon K. Kirchmayer Award on graduate teaching and mentoring, the IEEE Signal Processing Society 2014 Society Award, the IEEE Signal Processing Society 2009 Technical Achievement Award, the Highly Cited Researcher Award by Web of Science, the 2017 CEATEC Grand Prix award for his invention of time-reversal machine by Origin Wireless, Inc., the University-Level Invention of the Year Award from the University of Maryland the College-Level Poole and Kent Senior Faculty Teaching Award, the Outstanding Faculty Research Award, and the Outstanding Faculty Service Award from the A. James Clark School of Engineering, and over a dozen Best Paper Awards. He is an elected IEEE Vice President of Technical Activities. He was the President of the IEEE Signal Processing Society, where he has served as the Vice President of Publications and the Board of Governor, and a member of the IEEE Board of Director as the Division IX Director. He has also served as the Editor-in-Chief of *IEEE Signal Processing Magazine*. He is a Fellow of the AAAS.